

# **c-Axis Dimer Inducing Dome-like Superconductivity in Weakly Correlated RE<sub>2</sub>Cu<sub>5</sub>As<sub>3</sub>O<sub>2</sub> (RE=La, Pr)**

Xu Chen<sup>1,2,‡</sup>, Jiangang Guo<sup>1,‡,\*</sup>, Chunsheng Gong<sup>1</sup>, Erjian Cheng<sup>3</sup>, Congcong Le<sup>4,1</sup>, Ning Liu<sup>1,2</sup>, Tianping Ying<sup>3</sup>, Qinghua Zhang<sup>3</sup>, Jiangping Hu<sup>1,4,6</sup>, Shiyan Li<sup>3,5</sup>, Xiaolong Chen<sup>1,2,6,\*</sup>

Email: [jgguo@iphy.ac.cn](mailto:jgguo@iphy.ac.cn); [xlchen@iphy.ac.cn](mailto:xlchen@iphy.ac.cn)

1 Beijing National Laboratory for Condensed Matter Physics, Institute of Physics, Chinese Academy of Sciences, P. O. Box 603, Beijing 100190, China

2 University of Chinese Academy of Sciences, Beijing 100049, China

3 State Key Laboratory of Surface Physics, Department of Physics, and Laboratory of Advanced Materials, Fudan University, Shanghai 200433, China

4 Kavli Institute of Theoretical Sciences, University of Chinese Academy of Sciences, Beijing 100190, China

5 Collaborative Innovation Center of Advanced Microstructures, Nanjing 210093, China

6 Collaborative Innovation Center of Quantum Matter, Beijing 100190, China

**Abstract:** We report that the observation of superconductivity in new layered Cu-based compound RE<sub>2</sub>Cu<sub>5</sub>As<sub>3</sub>O<sub>2</sub> (RE=La, Pr). Resistivity and specific heat measurements reveal that it belongs to a weakly-correlated system. We show that  $T_c$  exhibits dome-like variation as substituting Cu by magnetic element Ni with maximum  $T_c$  of 2.5 K and 1.2 K in such systems. From the details of structure, we have been able to establish that the As-As dimer along the  $c$ -axis is formed, closely relating to the enhancement of superconductivity. Our results highlight the insensitivity to magnetic pairing breaking by magnetic ions and doping range in weakly-correlated system.

In superconductors, the disorder-induced pair breaking strongly relies on the specific physical mechanism, what can be viewed as an informative factor to study the details of gap symmetry. In weakly-correlated Bardeen-Cooper-Schrieffer (BCS) superconductors, non-magnetic impurity should not apparently decrease the superconducting transition temperature ( $T_c$ ), but the magnetic impurity with broken time reversal symmetry can break Cooper-pairs quickly.<sup>1</sup>

As for strong correlated superconductivity, such as *d*-wave cuprates, doping spacer layer or superconducting layer can bring out distinct properties. Dome-like  $T_c$  shows up when the content of dopants in spacer layer increases from 5% to 25%.<sup>2</sup> However, the non-magnetic elements (Zn) substitution on CuO<sub>2</sub> layer can suppress the  $T_c$  as strong as magnetic elements (Fe, Co, Ni) due to the formation of net magnetic moment on the Cu-O<sub>2</sub> plane.<sup>3</sup> This scenario is totally different from those of iron-pnictides superconductors, in which non-magnetic and magnetic impurity can induce high  $T_c$ . For example, antiferromagnetic metal BaFe<sub>2</sub>As<sub>2</sub> becomes superconducting as the Ba<sup>2+</sup> or As<sup>3-</sup> is substituted by K<sup>+</sup>/Na<sup>+</sup>/Rb<sup>+</sup> or P<sup>3-</sup>,<sup>4,5,6,7</sup> respectively. Surprisingly, the dome-like  $T_c$  can be achieved by substituting Fe<sup>2+</sup> by magnetic Co<sup>2+</sup> and Ni<sup>2+</sup> ions.<sup>8,9,10</sup> One explanation is that the doping is justified by the rigid-band model in some extent, where the doped electrons behaving itinerant states shift the Fermi level to the higher density of states, enhancing the  $T_c$ .<sup>11,12</sup> However, recent theoretical work argued that the extra *d* electrons are bounded to Co<sup>2+</sup> and Ni<sup>2+</sup> sites without doping carriers.<sup>13</sup>

Then, a question arises, if the superconductivity of weak correlation can be enhanced by magnetic ion. This question, undoubtedly, is of importance not only in exploration of new superconductor but also in understanding the superconducting mechanism. In this Letter, we report the synthesis and characterization of a kind of novel layered superconducting parent, RE<sub>2</sub>Cu<sub>5</sub>As<sub>3</sub>O<sub>2</sub> (RE=La, Pr), where Cu is coordinated by As in a new form Cu<sub>5</sub>As<sub>3</sub>. La<sub>2</sub>Cu<sub>5</sub>As<sub>3</sub>O<sub>2</sub> shows superconductivity at  $T_c$ =0.63 K while Pr<sub>2</sub>Cu<sub>5</sub>As<sub>3</sub>O<sub>2</sub> is non-superconducting phase. Strikingly, upon magnetic element Ni doping, higher  $T_c$  emerges in both RE<sub>2</sub>(Cu<sub>1-x</sub>Ni<sub>x</sub>)<sub>5</sub>As<sub>3</sub>O<sub>2</sub> compounds. Their crystal structures exhibit anomalous variation as approaching the highest  $T_c$ , which

can be attributed to the formation of As-As dimer along *c*-axis.

The synthetic details and characterization methods are summarized in Supplemental Materials (SM). Fig. 1(a) shows the HADDF image of (110) plane of  $\text{La}_2\text{Cu}_5\text{As}_3\text{O}_2$ , in which two kinds of slabs stack along the *c*-axis, indicating a typical layered structure. The collected powder X-ray diffraction (PXRD) pattern of  $\text{La}_2\text{Cu}_5\text{As}_3\text{O}_2$  can be indexed by a body-center tetragonal cell with space group *I*4/mmm (No. 139). The refined lattice constants are  $a=b=4.1386(1)$  Å and  $c=22.8678(6)$  Å. We construct the initial model by setting La1 4e (0.5, 0.5, *z*1), O1 4d (0.5, 0, 0.25), Cu(1) 8g (0.5, 0, *z*2), Cu(2) 2b (0, 0, 0.5), As(1) 4e (0, 0, *z*3) and As(2) 2a (0, 0, 0) as per *I*4/mmm. The Rietveld refinements successfully converge to  $R_p=2.95\%$ ,  $R_{wp}=4.26\%$  and  $\chi^2=3.87$ , and the refined results are shown in Fig. 1(b).  $\text{Pr}_2\text{Cu}_5\text{As}_3\text{O}_2$  is found to be isostructural to  $\text{La}_2\text{Cu}_5\text{As}_3\text{O}_2$  with lattice parameters  $a=4.0802(1)$  Å and  $c=22.9144(5)$  Å. The crystallographic parameters of  $\text{RE}_2\text{Cu}_5\text{As}_3\text{O}_2$  (RE=La, Pr) are listed in Table S1 of SM.

The crystal structure of  $\text{RE}_2\text{Cu}_5\text{As}_3\text{O}_2$  is drawn in Fig. 1(c), one can see that the  $\text{Cu}_5\text{As}_3$  blocks and the fluorite  $\text{Re}_2\text{O}_2$  layers stack along *c*-axis, which agrees with the atomic distributions in HADDF image and EDS analysis (Fig. S1, SM). Figure 1(d) is the structural detail of the  $\text{Cu}_5\text{As}_3$  block, where the cage can be viewed as replacing neighbor As(1)<sup>3-</sup> anions in two  $\text{Cu}_2\text{As}_2$  layers by one Cu atom. The bond lengths of Cu(1)-As(1) and Cu(1)-Cu(1) are 2.41 Å and 2.93 Å, respectively, close to the values in  $\text{BaCu}_2\text{As}_2$ .<sup>14</sup> It is noted that the bond length of As(1)-As(2), 2.81 Å, locates at the bonding regime of As-As covalent bond, 2.7~2.9 Å.<sup>15</sup>  $\text{Cu}_5\text{As}_3$  unit is analogous to  $\text{Cu}_6\text{Pn}_2$  in  $\text{BaCu}_6\text{Pn}_2$  ( $\text{Pn}=\text{As, P}$ ),<sup>16</sup> where the central As2 atom is replaced by one Cu atom. Partial metallic bonding Cu-Cu should exist as indicated by bond length of Cu(1)-Cu(2), 2.60 Å, see Fig. 1(e). Additionally, we note a distorted CuAs rectangle plane in the *xz/yz* planes, in which the bond lengths of Cu(1)-As(1) and Cu(1)-As(2) are 2.41 Å and 2.60 Å, respectively, see Fig. 1(f). In this plane, the ligand As *p* orbitals are not oriented directly towards the Cu(1) *d*<sub>xy</sub> orbitals, which will weaken the splitting magnitude of 3*d* orbitals of Cu(1).

The transport properties of both compounds are presented in Fig. 2. The electrical

resistivity show typical metallic behavior from 300 K to 1.8 K, which can be fitted by  $\rho \sim T^2$  at low temperature range, obeying the Fermi-liquid behavior, see Fig. 2(a) and Fig. S2. Resistivity kinks for  $\text{La}_2\text{Cu}_5\text{As}_3\text{O}_2$  and  $\text{Pr}_2\text{Cu}_5\text{As}_3\text{O}_2$  at  $T^* = 80$  K and 40 K can be observed, respectively. The external magnetic fields up to 9 T do not weaken the kinks. The magnetic susceptibility ( $\chi$ ), specific heat ( $C_p$ ) and PXRD patterns under low temperatures were measured to detect the origin of this transition. The analyses of  $\chi$  show that the magnetic moment is  $\sim 0.16\mu_B$ ,  $\theta = -148(1)$  K, implying an AFM interaction of Cu ions. The fitting of  $C_p$  gives Debye temperature  $\Theta_D$  is 169(2) K and Sommerfeld coefficient  $\gamma_0 = 5.01 \text{ mJ} \cdot \text{mol}^{-1} \cdot \text{K}^{-2}$  for  $\text{La}_2\text{Cu}_5\text{As}_3\text{O}_2$  (Fig. S3, SM). The kinks in  $\chi$  and  $C_p$  confirm the phase transition is bulky. The Rietveld refinements of temperature-dependent PXRD patterns of  $\text{La}_2\text{Cu}_5\text{As}_3\text{O}_2$  reveal that the  $c$ -axis monotonously decreases from 22.8678(6) Å to 22.7370(6) Å on cooling, but the  $a$ -axis firstly decreases to 4.1357(9) Å and slightly increases below 80 K, implying a tiny structural distortion of  $ab$ -plane without rotation symmetry breaking<sup>17</sup>, see Fig. S4, SM. We rule out the possibility of charge/spin density wave transition by measuring the TEM and neutron diffraction of  $\text{La}_2\text{Cu}_5\text{As}_3\text{O}_2$  at low temperatures, see Fig. S5, SM. Measuring the resistivity at very low temperature reveals that  $\text{La}_2\text{Cu}_5\text{As}_3\text{O}_2$  is a superconductor with  $T_c^{\text{onset}} = 0.63$  K and  $T_c^{\text{zero}} = 0.26$  K, as shown in Fig. 2(b). This transition is suppressed by external magnetic field and finally disappears as  $B > 0.12$  T. The upper critical fields  $\mu_0 H_{c2}(0)$ , 0.15 T and 0.18 T, are estimated from the linear and Ginzburg-Landau (GL) fitting, respectively (Fig. S6, SM). In contrast, the  $\text{Pr}_2\text{Cu}_5\text{As}_3\text{O}_2$  does not show superconducting transition above 0.25 K. This difference is possibly similar to the similar effect in suppressed superconductivity of Pr-based cuprates<sup>18,19</sup>.

We prepared a series of  $\text{RE}_2(\text{Cu}_{1-x}\text{Ni}_x)_5\text{As}_3\text{O}_2$  ( $x = 0-1.0$ ) samples so as to further explore the evolution superconductivity against magnetic element substitution. The electrical resistivity of  $\text{RE}_2(\text{Cu}_{1-x}\text{Ni}_x)_5\text{As}_3\text{O}_2$  at very low temperature are shown in Fig. 3(a) and (b). For  $\text{La}_2(\text{Cu}_{1-x}\text{Ni}_x)_5\text{As}_3\text{O}_2$ , the  $T_c^{\text{onset}}$  continuously increases from 0.63 K ( $x=0$ ) to the maximal 2.5 K ( $x=0.4$ ). It is emphasized that superconductivity can be induced in the non-superconducting  $\text{Pr}_2\text{Cu}_5\text{As}_3\text{O}_2$  upon doping Ni, in which the

highest  $T_c^{\text{onset}}$  are 1.2 K for  $\text{Pr}_2(\text{Cu}_{0.65}\text{Ni}_{0.35})_5\text{As}_3\text{O}_2$ . As  $x > 0.4$ , the  $T_c^{\text{onset}}$  gradually decreases to zero. The external magnetic field smoothly suppresses the superconductivity, and the  $\mu_0 H'_{\text{c}2}(0)$  are 3.8 T (3.0 T) and 0.69 T (0.52 T) estimated from the linear (GL) fitting, respectively (Fig. S7, SM). In Fig. 3(c), the magnetization of  $\text{La}_2(\text{Cu}_{0.6}\text{Ni}_{0.4})_5\text{As}_3\text{O}_2$  exhibits  $\sim 40\%$  superconducting volume fraction at 1.8 K, indicating a bulk superconductivity. Meanwhile, the bulk superconductivity of  $\text{La}_2(\text{Cu}_{0.6}\text{Ni}_{0.4})_5\text{As}_3\text{O}_2$  is further confirmed by a large superconducting jump in the specific heat ( $C_p$ ). The magnetic field up to 5 T could totally suppress the transition, as seen from Fig. 4(d). We fit the  $C_p(5\text{T})$  data using the equation  $C_p/T = \gamma + \beta T^2$ , and obtain the  $\gamma = 12.62 \text{ mJ}\cdot\text{mol}^{-1}\cdot\text{K}^2$ ,  $\beta = 9.89 \text{ mJ}\cdot\text{mol}^{-1}\cdot\text{K}^{-4}$  and  $\Theta_D = 133(2) \text{ K}$ . Extrapolating the data to 0 K finds a residual  $\gamma_n$  is  $1.58 \text{ mJ}\cdot\text{mol}^{-1}\cdot\text{K}^2$ , indicating that the non-superconducting phase is  $\sim 12.5\%$  due to impurity or finite states induced by scattering for a nodal gap. Thus we can obtain the superconducting  $\gamma_s$  is  $11.04 \text{ mJ}\cdot\text{mol}^{-1}\cdot\text{K}^2$ , which results in the dimensionless jump of  $C_e/\gamma_s T_c$  is 1.42. The value is consistent with the BCS weak-coupling limit (1.43), but smaller than that of the optimal K-doped  $\text{BaFe}_2\text{As}_2$  (2.5).<sup>20</sup> Figure 4(f) plots the semi-logarithmic of  $C_e/T$  as a function of temperature. We subtract the upturn of  $C_e/T$  at very low temperature due to Schottky anomaly using the treatment in Ref. [21] and obtain the flatten  $C_e/T$ . The detail of estimating the Schottky anomaly is shown in Fig. S8 (SM). As expected from the BCS theory,  $\ln(C_e/T) \propto -\frac{\Delta(0)}{k_B T}$ , the data in Fig. 3(f) are linearly fitted, yielding superconducting gap  $\Delta(0) = 0.23 \text{ meV} = 2.65 k_B \text{ K}$ . Knowing the  $\Delta(0)$ , a  $2\Delta(0)/k_B T_c$  is 2.58, which is smaller than the weak-coupling limit (3.52) within the BCS framework. Note that the subtracting of Schottky anomaly possibly undermines the rationality of *S*-wave superconductivity.

The PXRD confirms  $\text{RE}_2(\text{Cu}_{1-x}\text{Ni}_x)_5\text{As}_3\text{O}_2$  is a continuous solid solution, judging from the linear decrease in volume of unit cell (Fig. S9, SM). We carried out the Rietveld refinements for all PXRD patterns and listed the crystallographic parameters in Table S1. The selected crystallographic parameters are plotted in Fig. 4. One can see that the *a*-axis almost keeps constant and the *c*-axis decreases drastically as  $x < 0.4$ ,

however, this variation is reversed as  $x>0.4$ , see Fig. 4(a). This anomalous feature makes the  $c/a$  ratio initially decreases as  $x<0.4$  while it starts to increase as  $x>0.4$ , where the minimum shows up at  $x=0.4$  shown in Fig. 4(b). To our best knowledge, the structural change of  $a$ ,  $c$  and ‘V’ shape of  $c/a$  ratio is a rare case in layer superconductors. Fig. 4(c) and (d) show that the decreasing of Cu1-As1 distance and  $h_1$  show a crossover at  $x=0.4$ , however, we notice that the Cu1-As2 bond length and  $h_2$  (Fig. 4e) only show monotonous decrease upon Ni doping. The distinct response of  $h_1$  and  $h_2$  on Ni doping induces a crossover of the shrinking of As1-As2 bond length at  $x=0.4$ , see Fig. 4(f). We measured the neutron powder diffraction data of  $\text{La}_2\text{Cu}_3\text{Ni}_2\text{As}_3\text{O}_2$  ( $x=0.4$ ), and the best-fitting results indicate that the two Ni ions occupy the Cu1 site rather than random distribution, see Fig. S10, SM. Since the Cu2-As2 bond lengths ( $\sqrt{2}^*a/2$ ) almost keep a constant as  $x<0.4$ , it is rational to conclude that the Ni firstly occupies the Cu1 site, shortening the  $h_1$  and  $c$ -axis. As  $x>0.4$ , Ni ions seems substitute the Cu1 and Cu2 sites without preferred occupation.

The electrical resistivity of  $\text{RE}_2(\text{Cu}_{1-x}\text{Ni}_x)_5\text{As}_3\text{O}_2$  from 1.8 K-300 K shows that the  $T^*$  of  $\text{RE}_2\text{Cu}_5\text{As}_3\text{O}_2$  is rapidly suppressed upon Ni doping (Fig. S11, SM). In the Ni-rich samples, another resistivity anomaly shows up, which gradually increases to 260 K and 210 K for end-member  $\text{La}_2\text{Ni}_5\text{As}_3\text{O}_2$  and  $\text{Pr}_2\text{Ni}_5\text{As}_3\text{O}_2$ , respectively. We have measured the PXRD patterns of  $\text{La}_2(\text{Cu}_{0.02}\text{Ni}_{0.98})_5\text{As}_3\text{O}_2$  and  $\text{Pr}_2\text{Ni}_5\text{As}_3\text{O}_2$  samples from 300 K to 10 K. It is found that the (200) and (215) peaks split into (020)/(200) and (125)/(215) peaks below  $T_s$ , suggesting a structural symmetry breaking from  $C_4$  to  $C_2$  (Fig. S12, SM). The PXRD pattern of  $\text{La}_2(\text{Cu}_{0.02}\text{Ni}_{0.98})_5\text{As}_3\text{O}_2$  at 10 K can be indexed by an orthorhombic  $I$ -centered unit cell ( $I\text{mmm}$ , No.71) with  $a_0=4.0608(1)$  Å,  $b_0=4.0798(1)$  Å and  $c_0=22.3317(3)$  Å. The structural transition is also observed in  $\text{Pr}_2\text{Ni}_5\text{As}_3\text{O}_2$  (Fig. S13, SM).

The whole electronic phase diagram of  $\text{RE}_2(\text{Cu}_{1-x}\text{Ni}_x)_5\text{As}_3\text{O}_2$  are plotted in Fig. 5(a). One can find that dome-like  $T_c$  are observed, where the superconducting phases emerge at  $0< x < 0.6$  and  $0.2 < x < 0.45$  for  $\text{La}_2(\text{Cu}_{1-x}\text{Ni}_x)_5\text{As}_3\text{O}_2$  and  $\text{Pr}_2(\text{Cu}_{1-x}\text{Ni}_x)_5\text{As}_3\text{O}_2$ , respectively. The phase diagram is similar to those of cuprates and iron-based superconductors to large extent, which features the phase competition

characteristics. Furthermore, the enhancement of superconductivity upon doping magnetic ions is rare, which are only observed in iron-based superconductors<sup>22,23</sup>. There is a gap between the superconducting regime and the  $C_4$ - $C_2$  phase transition, implying the absence of direct competition of them.

We calculated the electronic structure in the paramagnetic state from DFT calculations. The band structures of  $\text{La}_2\text{Cu}_5\text{As}_3\text{O}_2$  are shown in Fig. 5(b), where a small hole-pocket and three large electron-pockets show up at the  $\Gamma$  and  $\text{M}$  point, respectively. Around  $E_F$ , the bands along the  $\Gamma$ - $\text{X}$  and  $\Gamma$ - $\text{Y}$  directions have large dispersion while the bands along  $\Gamma$ - $\text{Z}$  are almost flat, indicating that the Fermi surfaces are quasi-two-dimensional. The hole-pocket is mainly composed of Cu(1)  $d_{x^2-y^2}$  hybridizing with As(1)  $P_z$ , and the electron-pockets components are Cu(1)  $d_{xz}/d_{yz}$ ,  $d_{xy}$  and As(1)  $P_{x/y}$  [Fig. S14(a), SM]. It is noted that the orbitals  $d_{xz}/d_{yz}$  dominate the states at  $E_F$ , different from those in  $\text{CuO}_2$  plane and  $\text{FeAs}_4$  tetrahedron. In Fig. 5(c), one clearly sees that the  $E_F$  is dominated by Cu(1)  $d$  and As(1)  $p$  states, and the states of La and O mainly locate -5 eV to -3 eV [Fig. S14(b), SM]. The total  $N(E_F)$  is 1.75 states/eV f. u.. The bare Sommerfeld coefficient is 4.11  $\text{mJ mol}^{-1} \text{K}^2$ , which is close to the experimental  $\gamma_0$  of un-doped  $\text{La}_2\text{Cu}_5\text{As}_3\text{O}_2$  and comparable to that in the low-carriers-density  $\text{LaFeAsO}$ .<sup>24</sup> Figure 5(d) shows that the large Fermi surface around  $\text{M}$  point is oriented to the axes of momentum-space. The hole-pocket is small, so the main Fermi surface is electron-type.

It is previously reported that the bonded anionic dimer could induce ferromagnetic critical point, superconductivity and metal-insulator transition.<sup>25,26,27</sup> As mentioned above, there are weak bonding states of As(1)-As(2) in  $\text{RE}_2\text{Cu}_5\text{As}_3\text{O}_2$ , and the  $E_F$  will higher than the bonding orbital ( $\sigma$ ), and locates the bottom of the anti-bonding orbital ( $\sigma^*$ ).<sup>28,29</sup> In the  $x < 0.4$  range, the doped holes would firstly enter into the As(1)-As(2) bond and lift the valence of  $\text{As}^{3-}$ . The bonded apical As1 and central As(2) rapidly decreases the  $c$ -axis. At the same time, the  $E_F$  slowly drops to the energy between  $\sigma$  orbital and  $\sigma^*$  orbital as the As(1)-As(2) bond shortens. As  $x > 0.4$ , the shrinking of As(1)-As(2) bond length and  $c$ -axis slows and the  $a$ -axis begin to

decrease, means that some of excess holes are introduced the lattice, leading to the decrease of superconductivity.

In summary, the results provide evidence of a novel kind of Cu-based superconductor, whose  $T_c$  and crystal structure can be effectively tuned through magnetic Ni element. The dimerization of As-As bonds along  $c$ -axis and shrinking of  $a$ -axis in turn leads to a dome-like  $T_c$  even in weakly correlated superconductors. These findings in  $\text{Cu}_5\text{As}_3$ -based superconducting family provide an new perspective to explore new quantum properties in layered superconductors.

#### **ACKNOWLEDGMENT**

We acknowledge Profs. H. Ding, L. H. He and Y. Zhang for valuable discussions and TEM and neutron measurements. This work was supported by the National Natural Science Foundation of China (No. 51532010, 51772322), the National Key Research and Development Program of China (Project No. 2017YFA0304700, 2016YFA0300600), the Starting-up for 100 talent of Chinese Academy of Sciences, and the Strategic Priority Research Program and Key Research Program of Frontier Sciences of the Chinese Academy of Sciences (Grants No. XDB07020100 and No. QYZDJ-SSW-SLH013).

#### **References**

---

- [1] P. W. Anderson, *J. Phys. Chem. Solid.* **11**, 26-30 (1959).
- [2] B. Keimer, *et al.*, *Nature* **518**, 179- 186 (2015).
- [3] G. Xiao, *et al.*, *Phys. Rev. B* **42**, 8752 (1990).
- [4] M. Rotter, *et al.*, *Phys. Rev. Lett.* **101**, 107006 (2008).
- [5] S. Avci, *et al.*, *Phys. Rev. B* **88**, 094510 (2013).
- [6] S. Peschke, *et al.*, *Z. Anorg. Allg. Chem.* **640**, 830-835 (2014).
- [7] S. Jiang, *et al.*, *J. Phys.: Condens. Matter* **21**, 495701 (2009).
- [8] A. S. Sefat, *et al.*, *Phys. Rev. Lett.* **101**, 117004 (2008).
- [9] P. C. Canfield, *et al.*, *Phys. Rev. B* **80**, 060501(R) (2009).
- [10] N. Ni, *et al.*, *Phys. Rev. B* **82**, 024519 (2010).
- [11] V. Brouet, *et al.*, *Phys. Rev. B* **80**, 165115 (2009).
- [12] S. Ideta, *et al.*, *Phys. Rev. Lett.* **110**, 107007 (2013).
- [13] H. Wadati, *et al.*, *Phys. Rev. Lett.* **105**, 157004 (2010).
- [14] B. Saparov and A. S. Sefat, *J. Solid State Chem.* **191**, 213-219 (2012).
- [15] H. Yakita, *et al.*, *J. Am. Chem. Soc.* **136**, 846-849 (2014).
- [16] J. Dünner and A. Mewis, *J. Alloy and Compounds* **221**, 65-69 (1995).

---

- [17] Q. Huang, *et al.*, *Phys. Rev. Lett.* **101**, 257003 (2008).
- [18] X. L. Chen, *et al.*, *Phys. Rev. B* **51**, 16444 (1995).
- [19] X. L. Chen, *et al.*, *Z. Phys.* **88**, 1-4 (1992).
- [20] P. Popovich, *et al.*, *Phys. Rev. Lett.* **105**, 027003 (2010).
- [21] G. Mu, *et al.*, *Phys. Rev. B* **76**, 064527 (2007).
- [22] A. S. Sefat, *et al.*, *Phys. Rev. Lett.* **101**, 117004 (2008).
- [23] N. Ni., *et al.*, *Phys. Rev. B* **82**, 024519 (2010).
- [24] D. J. Singh and M. H. Du, *Phys. Rev. Lett.* **100**, 237003 (2008).
- [25] S. Jia, *et al.*, *Nat. Phys.* **7**, 207-210 (2011).
- [26] J. G. Guo, *et al.*, *J. Am. Chem. Soc.* **134**, 20001-20004 (2012).
- [27] P. G. Radaelli, *et al.*, *Nature* **416**, 155-158 (2002).
- [28] R. Hoffmann, and C. Zheng, *J. Phys. Chem.* **89**, 4175–4181 (1985).
- [29] R. Hoffmann, Solids and surfaces: a chemist's view of bonding in extended structures. (VCH, 1988)

---

Figure 1. (a) The HADDF image of (110) plane of  $\text{La}_2\text{Cu}_5\text{As}_3\text{O}_2$ . (b) The Rietveld refinements of PXRD pattern of  $\text{La}_2\text{Cu}_5\text{As}_3\text{O}_2$ . (c) The crystal structure of  $\text{RE}_2\text{Cu}_5\text{As}_3\text{O}_2$  ( $\text{RE}=\text{La, Pr}$ ). (d) The  $\text{Cu}_5\text{As}_3$  unit comes from the combination of two  $\text{Cu}_2\text{As}_2$  layers with replacing two As atoms by Cu(2) atom. One As(2) atom is encapsulated in the center. (e) The Cu network along  $b$  direction with metallic bonds between Cu(1)-Cu(2) (2.60 Å). (f) The CuAs rectangle planar coordination at  $yz$  plane.

Figure 2. (a) The normal-state electrical resistivity of  $\text{Re}_2\text{Cu}_5\text{As}_3\text{O}_2$  as a function of temperature from 1.8 K-300 K. The data below  $T^*$  can be fitted by Fermi-liquid quation. (b) The electrical resistivity of  $\text{La}_2\text{Cu}_5\text{As}_3\text{O}_2$  around superconducting transition range with external magnetic field.

Figure 3.(a, b) Superconducting transition of  $\text{RE}_2(\text{Cu}_{1-x}\text{Ni}_x)_5\text{As}_3\text{O}_2$  ( $\text{RE}=\text{La, Pr}$ ). It can be found that the  $T_c$  firstly increases to maximum and then decreases to zero as increasing  $x$ . (c) The superconducting volume fraction for  $x=0.4$  and  $\text{RE}=\text{La}$  sample with ZFC and FC model at 10 Oe. (d) The  $C_p/T$  as a function of temperature under 0 T and 5 T. (e) The semi-logarithmic of  $C_e/T$  of  $\text{La}_2(\text{Cu}_{0.6}\text{Ni}_{0.4})_5\text{As}_3\text{O}_2$  as a function of temperature.

Figure 4. The selected crystallographic parameters (a)  $a$  and  $c$ , (b)  $c/a$  ratio, (c) Cu1-As1 bond length, (d) As height ( $h_1$ ), (e) Cu1-As2 bond length and As height ( $h_2$ ), (f) As1-As2 bond length of  $\text{RE}_2(\text{Cu}_{1-x}\text{Ni}_x)_5\text{As}_3\text{O}_2$  a function of Ni content.

Figure 5. (a) The electronic phase diagram of  $\text{RE}_2(\text{Cu}_{1-x}\text{Ni}_x)_5\text{As}_3\text{O}_2$ . It can be seen that the  $T^*$  is suppressed and  $T_c$  is enhanced. The inset shows the schematic evolution of  $\text{Cu}_5\text{As}_3$  block against Ni doping. (b) The Cu(1) orbital-weighted band structures of  $\text{La}_2\text{Cu}_5\text{As}_3\text{O}_2$ . (c) The projected density of states plotted at the ranges of -2 eV to 2 eV. (d) The derived Fermi surfaces of  $\text{La}_2\text{Cu}_5\text{As}_3\text{O}_2$  shown as stereo-view manner. Three large electronic pockets are observed at M point. The high symmetry points are labeled in the first Brillouin zone.

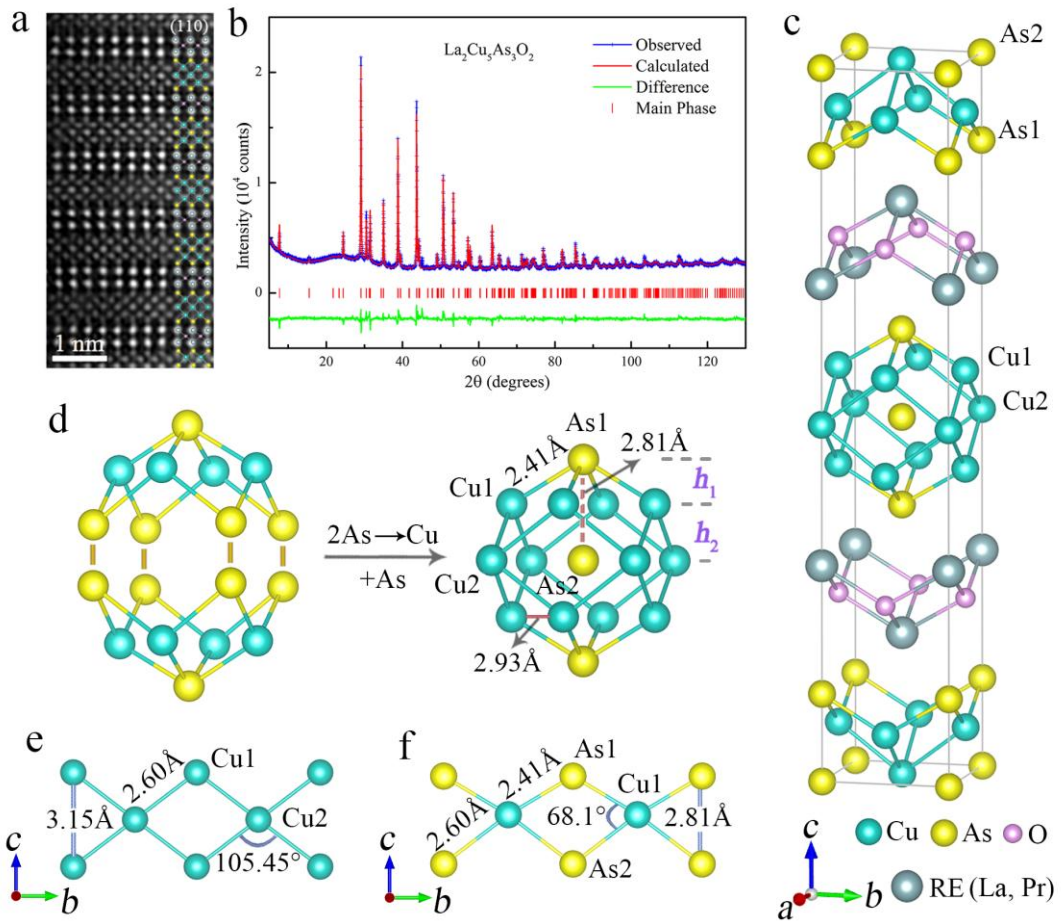


Figure 1. Chen *et al.*,

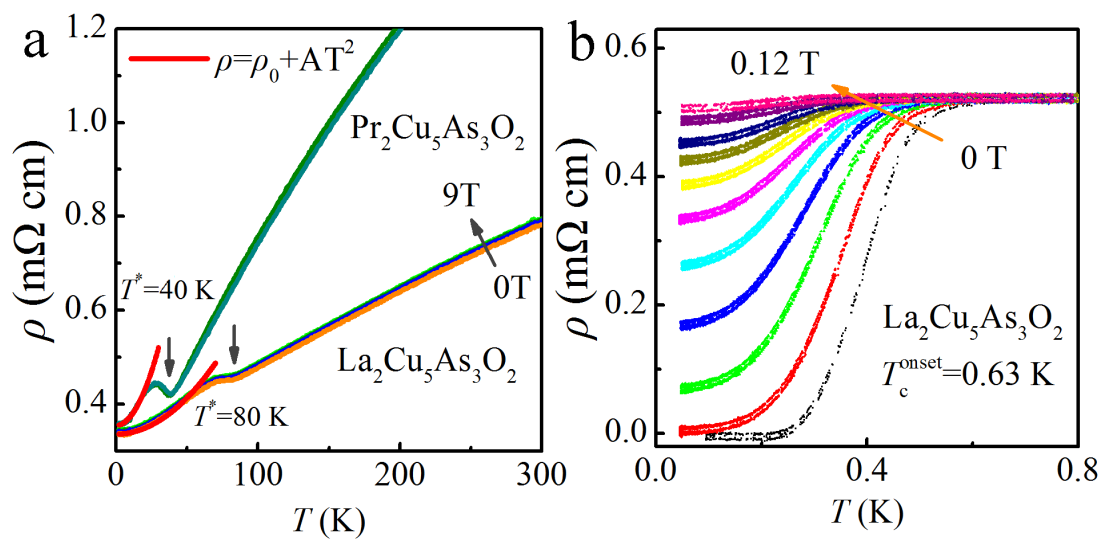


Figure 2. Chen *et al.*,

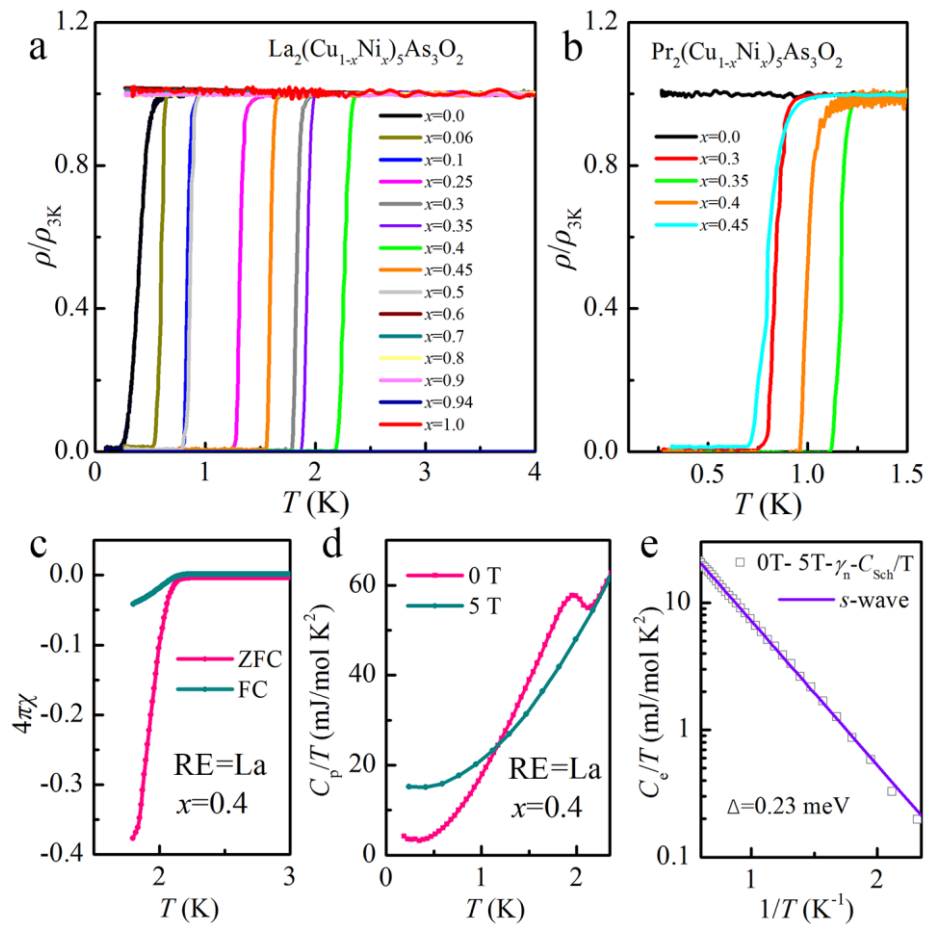


Figure 3. Chen *et al.*,

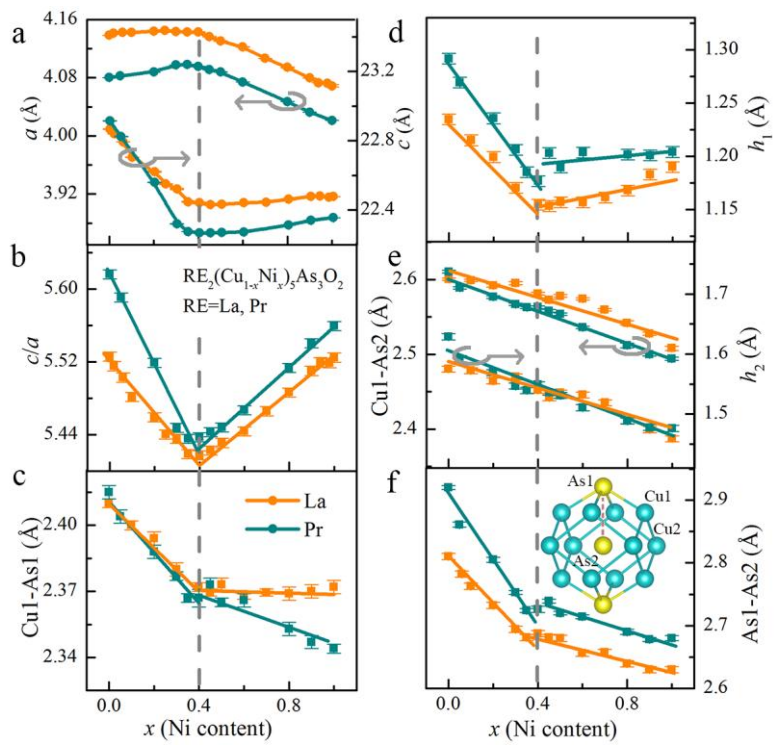


Figure 4. Chen *et al.*,

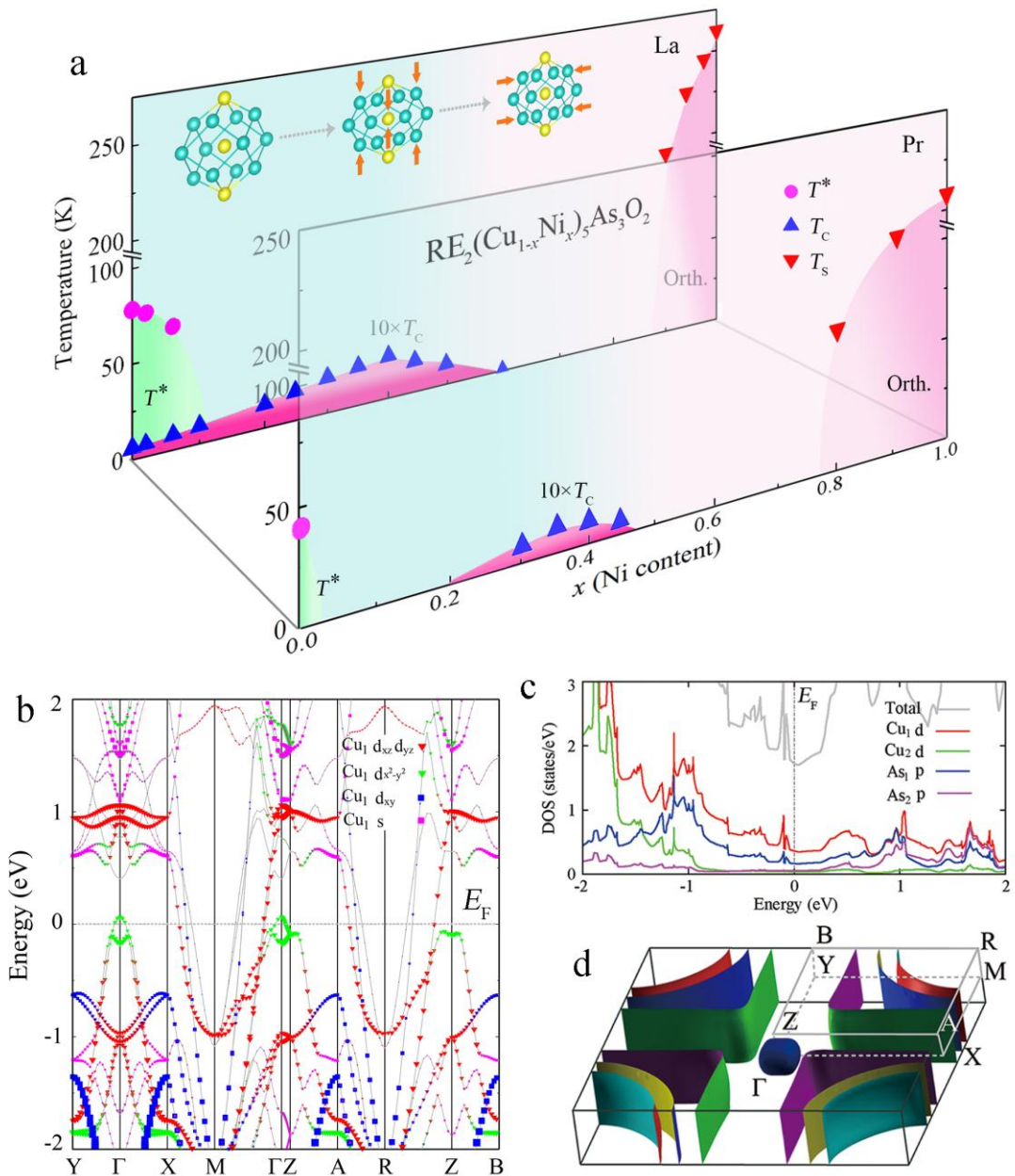


Figure 5. Chen *et al.*,